ELSEVIER

Fusion Engineering and Design 49–50 (2000) 605–611

Fusion Engineering and Design

www.elsevier.com/locate/fusengdes

Numerical and experimental prediction of the thermomechanical performance of pebble beds for solid breeder blanket

Zi Lu *, Alice Y. Ying, Mohamed A. Abdou

Mechanical and Aerospace Engineering Department, UCLA, Los Angeles, CA 90095-1597, USA

Abstract

In this paper, recent numerical modeling and experiment work for predicting the effective thermal and mechanical properties of solid breeder blanket pebble bed materials is presented. The numerical modeling is based on the micro-mechanics displacement method in conjunction with an iterative process of successive releasing of the contact force of particles. Initial and final packed states for particle assembly and the contact forces for particles have been studied. In addition, a test article has been constructed to measure the thermal stress induced by the thermal expansion of the solid particle and to estimate the characteristic properties of particle materials. Corresponding experiments are carried out with aluminum and Li_2ZrO_3 pebble beds. Empirical correlations for the moduli of deformation are presented. These experiment data are compared with the numerical modeling results.

Keywords: Thermomechanical performance; Pebble beds; Solid breeder blanket

1. Introduction

In many of the fusion reactor blanket designs, pebble beds have been proposed for tritium breeding and energy conversion as well as neutron multiplication. The packed beds must be stored in a structural container to keep the whole shape and design integrity. During the reactor operation, the bed will undergo thermal expansion relative to the container due to their substantial temperature differences and the irradiation swelling of particles. The maximum wall stress generated in the container is clearly an important design parameter, and the maximum contact force between any two particles will control attrition or break up of the particle materials. On the other hand, the increase in the contact areas between particles will lead to better effective thermal conductivity of pebble beds and probably different temperature profiles.

The distinct element method (DEM) developed by Cundall [1,2] has been successfully applied to analyses of granular assemblies. DEM is highly effective in case of rapid granular flow or time-de-

* Corresponding author. Tel.: +1-310-8258824; fax: +1-310-8251715.

E-mail address: zlu@fusion.ucla.edu (Z. Lu).

0920-3796/00/$ - see front matter
PII: S0920-3796(00)00348-3

pendent processes. But its disadvantages appear when equilibrium is needed — displacements are usually over-estimated and the calculated state oscillates around the exact solution. Kishino [3] published a model similarly to DEM; the algorithm calculates the displacements of each grain independently of the others, but the grains are displaced according to stiffness of the contacts with neighboring elements. Serrano and Rodriguez-Oritiz [4] built a quasi-static model based on the compilation of global stiffness matrix. This method has the disadvantage of major computational effort on rearranging and reformulating the global stiffness matrix for the contacts, whenever any new contact is formed or an old one disappears. On the other hand, experiments using photo elastic rods have also been performed by Oda et al. [5,6]. These experiments produced results on the relationship of stress tensor and contact normal distributions. Relationship between bulk behavior and packing structure under small strain conditions has been measured using a directional shear cell [7]. The stress-strain behaviors of the solid breeder blanket particle bed materials have been studied experimentally to evaluate the maximum stress levels to which bed particles and container wall are subjected [8,9].

In a pebble bed assembly, forces or heat flux are typically transferred through the contacts between particles. It is difficult to quantify the thermal and mechanical properties of pebble beds in details and precisely based only on continuum models — the transformation from a complicated discrete system to a simpler continuum system, results in certain information being lost. To remedy this deficiency, new discrete numerical models have been developed to simulate the thermal and mechanical properties of particle materials [10,11]. In this article, further results of the numerical modeling and experiments from UCLA are presented. Initial and final packed states for particle assembly and the contact forces for particles have been studied. The thermal stress induced by the thermal expansion of the pebble bed relevant to the structural container is experimentally measured. Empirical correlations for the bed effective moduli of deformation of particle materials are given. The experiment data is used to benchmark the numerical modeling results.

2. Numerical simulation

2.1. Numerical model

The detailed description of the numerical model is given in [11]. Basically it is a quasi-static model and no time-effects are considered. The particle bed is modeled as a collection of rigid particles interacting via Hertz type normal contact force and Coulomb's tangential friction force [12–14]. An iterative calculation of successive releasing of the forces exerted on a single particle is performed until the resultant force on each particle in assembly is sufficiently small — assembly reaches its equilibrium state. This discrete numerical model is more flexible in application and can provide essentially any desired piece of information (particle contact force, detailed micro-mechanical statistics, and particle spatial distributions) at any time that is not available in real physical experiments.

To simulate the practical distribution of particle size, the particle radius is varied by using two random numbers from a random number generator as follows: if the particle radius is RR initially, the actual particle radius is given by

$$R = \mathrm{RR}*(1 + \mathrm{pr}*\mathrm{RAND1} - \mathrm{pr}*\mathrm{RAND2}) \qquad (1)$$

where the RAND1 and RAND2 are two distinct random numbers each ranging from 0.0 to 1.0, pr ($0 \le \mathrm{pr} \le 1.0$) is a parameter to control the range of particle size. If $\mathrm{pr} = 0$, the assembly only has uniform size particle of radius RR, and if $\mathrm{pr} = 1.0$, the particle radius ranges from 0.0 to 2.0 RR. Fig. 1 shows the particle size distribution of an assembly with 10 000 particles ($\mathrm{pr} = 0.03$, $\mathrm{RR} = 0.5$ mm). It is very close to the Gaussian distribution.

The program automatically generates the initial particle assembly. As input data, the total particle number and the thermal and mechanical properties of solid particulate material are given, as well as the parameter to control the particle size range. The sizes of assembly volume and the minimal and maximal particle radii are calculated or recorded during the assembly generation process. The particle locations are given approximately according the orthorhombic packing initially — which mostly is not an equilibrium state for as-

sembly with different particle sizes (Fig. 1). Then the program searches for an equilibrium state of this assembly. As a result, an assembly consisting of touching particles in equilibrium is obtained. This state is taken as the initial equilibrium state for following loading and temperature rises.

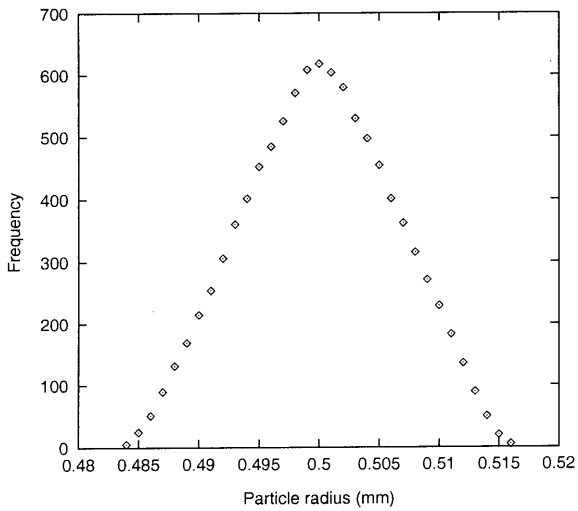

Fig. 1. Distribution of particle size for 10 000 particles.

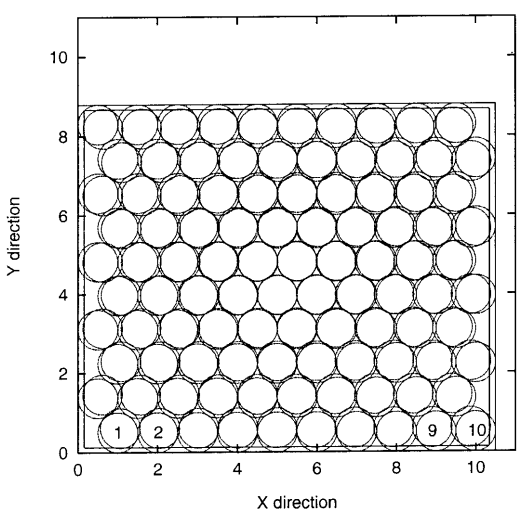

Fig. 2. Initial and final packed states under a hydrostatic compressive strain of 3% for a packed assembly using uniform particle size of 0.5 mm.

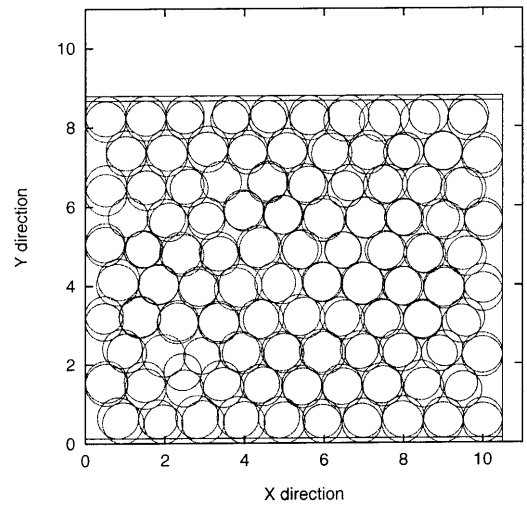

Fig. 3. Initial and final packed states under a uniaxial compressive strain of 3% for a packed assembly using a range of particle sizes between 0.5498 and 0.4518 mm.

2.2. Numerical simulation results

The assembly is assumed to be bounded by six rigid walls that form a cubic volume. The loading is controlled by strain or by moving the boundary elements according with the corresponding strain. The boundary elements are moved symmetrically with respect to the central axes of the particle assembly. The relative overlap at the particle contact point due to thermal expansion is given as

$$\delta = R_i(1 + \alpha\Delta T_i) + R_j(1 + \alpha\Delta T_j) - D_{ij} \quad (2)$$

where D_{ij} is the distance between two particles (counted from the centers), α the coefficient of thermal expansion of solid particle material, R_{ij} the particle radius, and ΔT_{ij} the corresponding particle temperature rise. The final particle position, contact forces, and macro-stresses are calculated after the equilibrium of assembly is reached. Depending on the procedure, next load and corresponding stresses may be taken and calculated.

Fig. 2 shows Initial and final packed states under a hydrostatic compressive strain of 3% for a packed assembly using uniform particle radius of 0.5 mm. Whereas the initial and final packed states under a uniaxial compressive strain of 3% for a packed assembly using a range of particle

radius between 0.5498 and 0.4518 mm is shown in Fig. 3. We can see that for a regular packed dense assembly of uniform size particle, the particles move only in the loading direction under hydrostatic or uniaxial compression—the strain field in the particle assembly is uniform (Fig. 2). Conversely, the particle moves in different directions if the bed is randomly packed initially and particle sizes have some ranges (Fig. 3) — the corresponding strain field is not uniform even if the external loading is uniform (uniaxial compression). This is particularly noticeable for particles located next to the boundary. These results point out that the deformation of particle material comes from the rearrangement of each particle as well as local elastic deformation at contact points. Consequently, a portion of the deformation is plastic deformation and is irreversible if the external loads are removed.

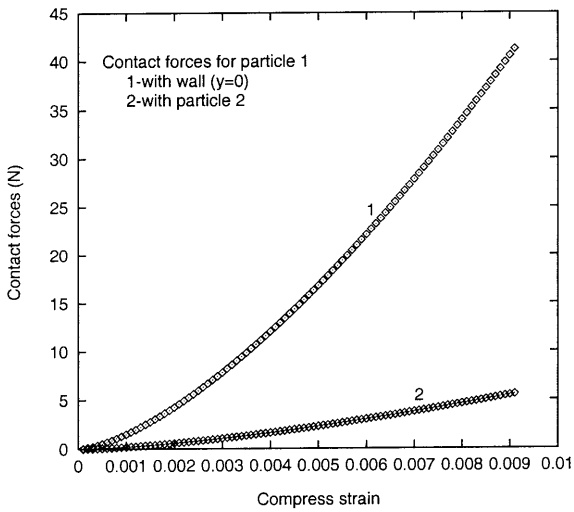

Fig. 4. Contact forces for particle 1 under a hydrostatic compressive strain of 1% for a packed assembly using uniform particle size of 0.5 mm.

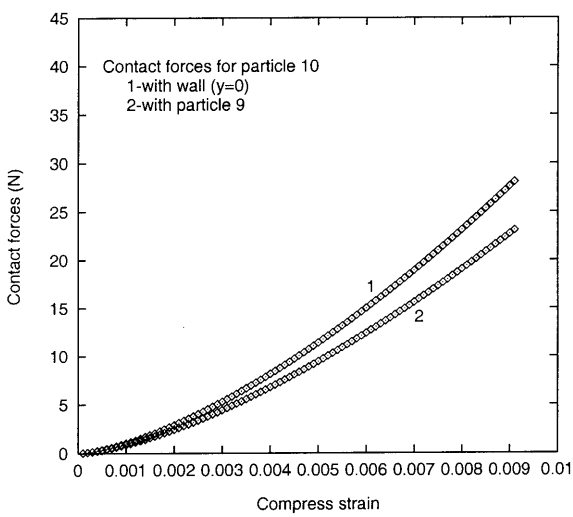

Fig. 5. Contact forces for particle 10 under a hydrostatic compressive strain of 1% for a packed assembly using uniform particle size of 0.5 mm.

Fig. 4 shows the contact forces for particle 1 with particle 2 and the structure wall, while Fig. 5 shows the contact forces for particle 10 with particle 9 and the structure wall (see Fig. 2 for detailed particle locations), respectively. Those contact forces increase with the increase of external hydrostatic load, but they do not have a linear relationship, which corresponds to the non-linear relationship between the normal Hertz contact force and the particle overlap δ. It is important to note that, though both particles are boundary elements only with different packing patterns, the contact forces are quite different. It means that the effective thermal conductivity of pebble bed changes from place to place, since the particle contact areas vary at different places due to the changing contact forces.

3. Physical experiment

3.1. Test apparatus

The investigated geometry of the test apparatus is shown in Fig. 6. A cylindrical particle bed sample (with diameter D_0 of 5.0 cm and height h of 1.3 cm) is confined in a stainless steel container. The outside structure frame applies an initial axial force F_{initial} on the particle bed through two pistons in the axial direction. Initially, the particle bed and cylindrical container are at the same uniform temperature T_{initial}. During the experiment, the particle bed's temperature will be raised to a homogeneous temperature, T_{final}, and the temperature rise is $\Delta T = T_{\text{final}} - T_{\text{initial}}$. The outside frame, far away from the container, always

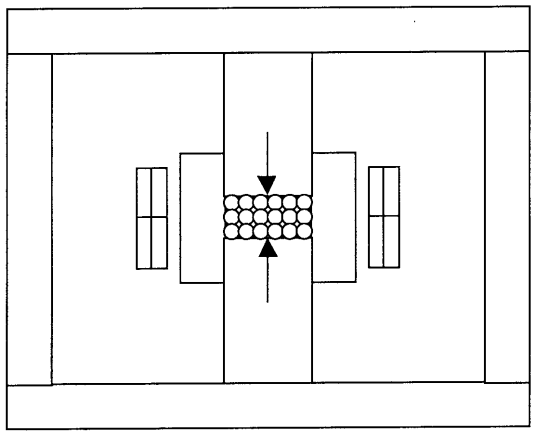

Fig. 6. Test article configuration.

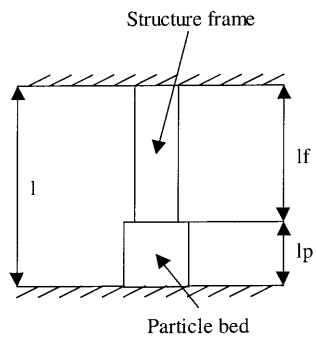

Fig. 7. Simplified test article model.

maintains at temperature $T_{initial}$. Due to thermal expansion of particle material and the constraint from the outside frame that is always at the initial temperature $T_{initial}$, thermal stress will occur and total force changes to F_{final}. The axial force change is $\Delta F = F_{final} - F_{initial}$. A force transducer measures the axial force. Based on ΔT and corresponding ΔF, the thermomechanical properties of corresponding particle materials are estimated.

3.2. Analytical model

The structure of Fig. 6 is equivalent to the simplified structure of Fig. 7: two rigid walls limit the thermal expansions of the particle bed and the outside frame. Initially at temperature $T_{initial}$, the total length is

$$l_f + l_p = l_{total} \tag{3}$$

where l_f and l_p are the initial frame length and length of particle bed sample, respectively. After the temperature is raised to T_{final}, the structure frame and the particle bed lengths will increase by Δl_{ft} and Δl_{pt}. Due to the induced thermal stress (compression), their lengths will decrease by Δl_{fs} and Δl_{ps}. The total length is still l_{total}, so that

$$l_f + \Delta l_{ft} - \Delta l_{fs} + l_p + \Delta l_{pt} - \Delta l_{ps} = l_{total} \tag{4}$$

Combine Eqs. (3) and (4), then

$$\Delta l_{ft} + \Delta l_{pt} = \Delta l_{fs} + \Delta l_{ps} \tag{5}$$

Eq. (5) shows that the decreased lengths, due to the compressive thermal stress, offset the increased lengths due to the thermal expansion — the total length remains the same.

The temperature rise in the particle bed is uniform so that Δl_{pt} is a linear function of ΔT. During the experiments, the frame is in the elastic range. The Δl_{fs} is linear function of ΔF. Combining all together

$$\Delta l_{ft}(\Delta T) + \alpha_p \Delta T l_p = [k_f l_f + k_p(\Delta F) l_p]\Delta F \tag{6}$$

where k_f and k_p are the stiffness coefficients for structure frame and particle bed sample, respectively, and α_p is the coefficient of thermal expansion of particle material. The $k_f l_f$ can be treated as one coefficient. To calibrate the $k_f l_f$, a small jack is used to replace the pebble bed sample with the same height. Changing the axial force by adjusting the jack, the relative displacement of two pistons is recorded. Based on the ratio of the axial force and corresponding displacement, the $k_f l_f$ is calibrated as 3.12×10^{-8} (m/N). To obtain $\Delta l_{ft}(\Delta T)$, the pebble bed are replaced with solid materials with known properties (304SS or Al). Then raising the temperature of the solid piece and frame, and monitoring the axial force change ΔF, the $\Delta l_{ft}(\Delta T)$ can be calculated for different temperature from Eq. (6). After calibrating the $\Delta l_{ft}(\Delta T)$ and $k_f l_f$ of the structure frame, the stiffness coefficient of particle bed, k_p, can be calculated based on Eq. (6) — assuming the coefficient of thermal expansion of particle material, α_p, is the same as that of solid material. Then the effective modulus of particle bed can be obtained as

$$E_p = \frac{1}{k_p A}(1 - 2v_p k_0) \quad (7)$$

where A is the area of the particle bed, v_p is the effective Poisson's ratio (0.05–0.25) and k_0 the coefficient of lateral pressure of particle material — 0.34 for most brittle ceramic pebble beds [15].

3.3. Experimental data and its comparison with numerical simulation

All experiments are carried out at $\Delta T = 43.4$°C (approximately from 24 to 68°C). The initial force stays around 4.4 (KN) which corresponds to 2.1 (MPa). The variations of axial force during the thermal cycles are shown in Fig. 8 for aluminum and ceramic (Li_2ZrO_3) particle beds. This figure demonstrates that for the first few cycles, the initial axial forces (at 24°C) drop a lot for both Al and the ceramic particle. This shows that the deformation of the particle bed is a consequence of the displacement of the particles and is irreversible. The number of cycles required to produce resilient conditions varies for aluminum and ceramic particle assemblies. However, the stress-strain relationship should become very stable within the first 50 cycles. Fig. 8 shows that, resilient conditions can be substantially formed during the first two (aluminum) or three (ceramic) cycles. Variation of the thermal forces with thermal cycles, including the effects of the thermal expansion of both structure frame and particle bed, is shown in Fig. 9. It is interesting to notice that the thermal force increases slightly with the thermal cycles for the aluminum pebble bed. Conversely, for ceramic pebbles, the thermal force decreases slightly with the thermal cycles. It shows that it is a consolidation process for the aluminum particle bed (denser and stiffer). Whereas the breakage of some ceramic particles cause the drops in the thermal stresses. At the end of experiments, broken ceramic particles are observed.

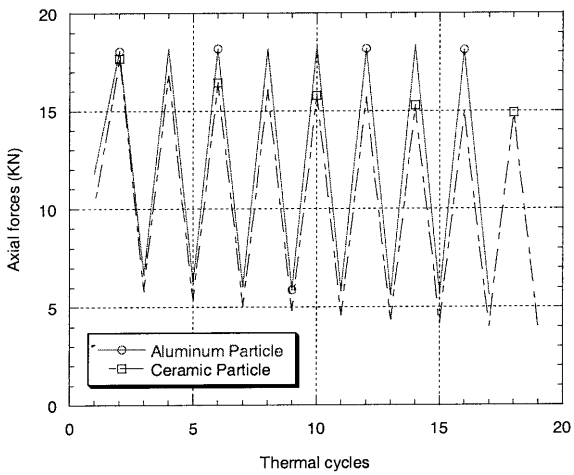

Fig. 8. Variation of axial forces during thermal cycles.

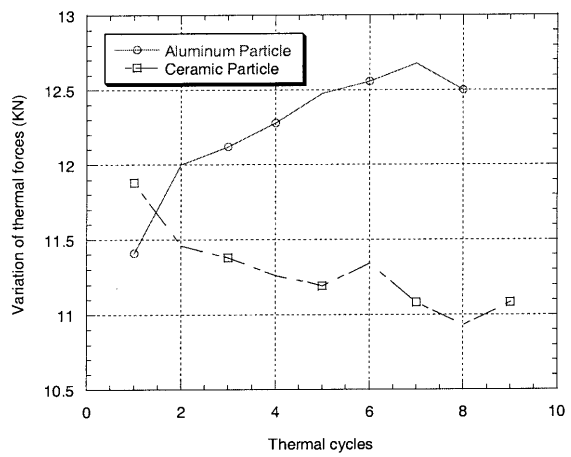

Fig. 9. Variation of the thermal forces with thermal cycles — including the effects of the thermal expansion of both structure frame and particle bed.

The calculated effective moduli of deformation, E_p, as a function of thermal cycles, are shown in Fig. 10 for aluminum and ceramic (Li_2ZrO_3) particle beds, respectively. Their trends are similar to that of thermal stresses. The average modulus of deformation is 0.175 (GPa) for the aluminum pebble bed, and 0.121 (GPa) for the ceramic (assuming a Poisson's ratio of 0.25, and a coefficient of lateral pressure 0.34). These moduli are much smaller than that of solid material that is consistent with prediction [15,16] and are very similar to the previous experiment results [8]. Fig. 10 also shows the numerical simulation results of the variation of effective modulus of deformation with thermal cycles for an aluminum particle bed. The numerical simulations are quite in line with the experiment data. Due to the brittleness of

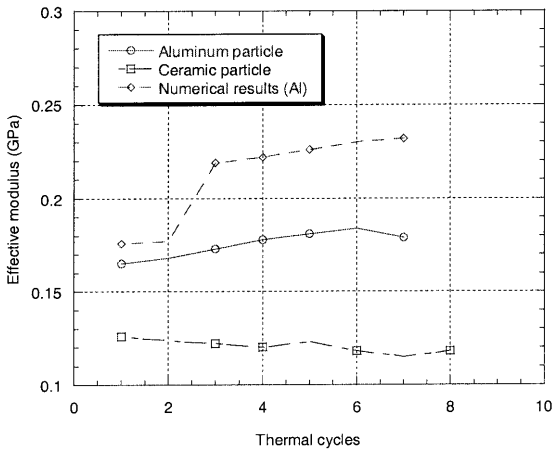

Fig. 10. Effective modulus of the particle assembly with thermal cycles.

ceramic pebble and corresponding breakage of particle during the experiments, there is large error between the simulations and experiments. Further development of the numerical model will incorporate the characteristic of the brittle of the ceramic particles.

4. Summary

To investigate the interaction between the ceramic breeder, beryllium pebble beds, and the structural materials in the cyclic operation of fusion reactor blanket, the characteristic properties of solid breeder blanket particle bed materials have been studied through numerical simulations and real physical experiments. A test article has been constructed to measure the thermal stress induced by the thermal expansion of the solid particle relevant to the structural container and to benchmark the discrete numerical model developed. The numerical simulations compare quite well with the experiment data. At present, the obtained data are far from complete and further numerical simulations and experiments are required.

References

[1] P.A. Cundall, O.D.L. Strack, A discrete numerical model for granular assemblies, Geotechnique 29 (1) (1979) 47–65.
[2] P.A. Cundall, Computer simulation of dense sphere assemblies, in: M. Satake, J.T. Jenkins (Eds.), Micro-Mechanics of Granular Materials, (Proc. US/Japan Seminar, October 26–30, 1987), Elsevier, Amsterdam, 1988, pp. 113–123.
[3] Y. Kishino, Disc model analysis of granular media, in: M. Satake, J.T. Jenkins (Eds.), Micromechanics of Granular Materials, Elsevier, Amsterdam, 1988, pp. 143–152.
[4] P.A. Serrano, J.M. Rodriguez-Ortiz, A Contribution to the Mechanics of Heterogeneous Granular Media, Proc. Symp. Plasticity and Soil Mechanics, Cambridge, 1973, pp. 215–228.
[5] M. Oda, J. Konishi, Microscopic deformation mechanism of granular material in simple shear, Soil Foundation 14 (1974) 25–38.
[6] M. Oda, J. Konishi, Nemat-Nasser, Some experimentally based fundamental results on the mechanical behavior of granular materials. Geotechnique 30 (1980) 479–495.
[7] C.S. Chang, A. Misra, Theoretical and experimental study of regular packings of granuales. J. Eng. Mechanics 115, 704–720.
[8] A. Ying, Z. Lu, M.A. 'Abdou, mechanical behavior and properties of solid breeder blanket packed beds', presented at ISFNT-4, Tokyo, Japan, April (1997). Fusion Eng. Design, in press.
[9] A. Ying, M.A. Abdou, 'Analysis of thermomechanical interactions and properties of ceramic breeder blankets,' presented at ISFNT-4, Tokyo, Japan, April (1997). Fusion Eng. Design, in press.
[10] M.A. Abdou, A. Ying, Z. Lu, Numerical Derivation of Thermal and Mechanical Properties of Ceramic Blanket Particle Bed Materials, presented at ICFRM-8, Sendai, Japan, October (1997). J. Nuclear Materials, in press.
[11] Z. Lu, A. Ying, M.A. Abdou, 3-D Numerical Simulation of Ceramic Breeder Blanket Pebble bed Thermomechanics-Methodology and Preliminary Results, presented at CBBI-8.
[12] K.L. Johnson, Contact Mechanics, Cambridge University Press, London, 1985.
[13] R.D. Mindlin, Compliance of elastic bodies in contact, J. Appl. Mechanics 16 (1949) 259.
[14] R.D. Mindlin, H. Deresiewicz, Elastic spheres in contact under varying oblique forces, J. Appl. Mechanics 20 (1953) 327.
[15] J. Feda, Mechanics of Particulate Materials — The Principles, Elsevier, New York, 1982.
[16] K. Walton, The effective elastic modulus of a random packing of spheres, J. Mech. Phys. Solids 35 (2) (1987) 213–226.